13 March 1998

ELSEVIER

Chemical Physics Letters 285 (1998) 105–113

CHEMICAL PHYSICS LETTERS

A non-adiabatic calculation of NO Rydberg states above several ionisation thresholds

Ismanuel Rabadán [a], Jonathan Tennyson [a,1], Lesley A. Morgan [b]

[a] *Department of Physics and Astronomy, University College London, Gower Street, London WC1E 6BT, UK*
[b] *Computer Centre, Royal Holloway, University of London, Egham, Surrey TW20 0EX, UK*

Received 13 November 1997; in final form 29 December 1997

Abstract

An ab initio study of the *ns*, *np*, *nd*, *nf* and *ng* Rydberg series of NO above a number of ionisation thresholds is presented. Calculations of the eigenphase sum of electron scattering by NO^+, using a non-adiabatic **R**-matrix method, are used to obtain vibrationally resolved positions and widths of NO autoionizing states. The complex quantum defects of the resonances are used to identify the Rydberg series, and these are separated according to the vibrational state of the target. Comparisons are made with experimental studies of this system. © 1998 Elsevier Science B.V.

1. Introduction

Rydberg states of molecules have excited much recent experimental interest, stimulated in part by the development of sensitive spectroscopic techniques which probe these high-lying electronically excited states. NO is particularly favoured for studies of this kind due to its high ionisation potential and the high electronic excitation energy of NO^+. It has thus become the benchmark molecule for many experimental studies. Some of the Rydberg states of NO lie in its continuum and a number of experimental studies have concentrated on their rotational and vibrational autoionisation [1–6]. Vibrational autoionisation is a process that arises through the coupling of the electronic and nuclear motion in the molecule and, consequently, relies in the breakdown of the Born-Oppenheimer approximation. Furthermore, Rydberg states also interact with valence states. This leads to competition between autoionisation and predissociation [7,8].

Theoretically Rydberg states of NO also make a good benchmark since the NO^+ core has a closed shell. However there has been considerably less theoretical work. Autoionisation of NO Rydberg states has been studied using multichannel quantum defect theory (MQDT) [8,9], but we are not aware of any direct ab initio calculations besides our own [10,11].

In this work, we present results on vibrational resolved autoionizing Rydberg states of NO between the $v^+ = 0$ and $v^+ = 5$ vibrational states of $NO^+(X\,^1\Sigma^+)$. This is done by using the **R**-matrix method to investigate the elastic scattering of electrons by NO^+.

2. Theory

We employ the UK molecular **R**-matrix package [12]. In this implementation, the coupling between

[1] E-mail: j.tennyson@ucl.ac.uk.

PII S0009-2614(98)00004-9

nuclear and electronic motions is included in the model through a non-adiabatic approximation [13] introduced by Schneider et al. [14]. This approximation takes, as starting point, the **R**-matrices at several internuclear distances. These were calculated by us previously [11]. The **R**-matrices were obtained using a close-coupling expansion that included the 12 lowest NO^+ target states which were represented using a configuration interaction (CI) expansion. Inside the (15 a_0) R-matrix sphere, the continuum was represented using (60σ, 57π, 54δ) numerical functions; further terms were added to the CI expansion to account for correlation and orthogonality relaxing effects. Full details of the construction of the target, continuum and system wavefunctions can be found in [11].

The implementation of the non-adiabatic **R**-matrix method has been described by Gillan et al. [13], so we only summarise the main ideas. As in the 'fixed-nuclei' **R**-matrix method, configuration space is partitioned in two regions. The internal region is the hypersphere defined by $0 \le r \le a$ and $A_{in} \le R \le A_{out}$, being r the coordinate of the scattering electron and R the internuclear distance. A_{in} is used to exclude the singularity of the nuclear repulsion and A_{out} is big enough so the vibrational functions considered have negligible amplitude for $R \ge A_{out}$.

In the internal region, the Hamiltonian ($\mathscr{H}$) includes the nuclear kinetic energy operator (T_R), the electronic Hamiltonian of the $N+1$ system (H_{N+1}) and the Bloch operator (L_{N+1}) to ensure Hermiticity. This Hamiltonian is diagonalized in the basis

$$\theta_k = \sum_{ij} \Psi_i(R_0)\,\xi_j(R)\,\gamma_{ijk} \qquad (1)$$

where Ψ_i is the fixed-nuclei electronic wavefunction [11] and ξ_j is a set of Legendre polynomials, 75 in this work, used to describe the nuclear motion. This basis is diabatic because it does not diagonalise H_{N+1} (except at $R = R_0$) but has the advantage of commuting with T_R, which greatly simplifies the diagonalisation of $\mathscr{H}$ [13].

In the external region, the wavefunction is expanded as:

$$\theta = \sum_{ijv} \phi_i r_{N+1}^{-1} F_{iv}(r_{N+1})\, Y_{l_j m_j}(\hat{\mathbf{r}}_{N+1})\, \chi_{iv}(R) \qquad (2)$$

where ϕ_i are the target electronic channels, χ_{iv} the target vibrational channels and F_{iv} monoelectronic radial functions. The matching of the internal and external wavefunctions in the hypersphere surface and the use of the asymptotic boundary conditions in F_{iv}, as in the standard **R**-matrix method, leads to the calculation of the collisional parameters and, in particular, the eigenphase sum.

The potentials for the nuclear motion are provided by the **R**-matrix poles calculated in [11]. 14 geometries are included in the calculation with R between $A_{in} = 1.606$ and $A_{out} = 2.835$ a_0.

The inner region calculation included 12 target states, but only the NO^+ ground state is retained in the outer region. This produces negligible differences in the position and autoionisation widths of the Rydberg states, as demonstrated in [11]. However, predissociation widths of Rydberg states requires interaction with valence states and the inclusion of the nuclear continuum in the calculation. This is possible in the **R**-matrix formalism but would required further calculations that we have not attempted.

The vibrational states of the target, χ_{iv}, are obtained using the program LEVEL [15]. This solves numerically the radial Schrödinger equation in the ab initio $NO^+(X\,^1\Sigma^+)$ potential of [11]. The vibrational thresholds obtained are given in Table 1; they agree within a few meV with experimental photoionisation data [6].

In this work, we calculate eigenphase sum for energies between the levels $v = 0$ and $v = 5$ of $NO^+(X\,^1\Sigma^+)$ (0 to 1.36 eV). Resonances in the eigenphase sum have been fitted to a Wigner-Breit profile using the program RESON [16] to obtain their position (E_r) and width (Γ). The complex quantum defects ($\mu = \alpha + i\beta$) of MQDT theory

Table 1
Vibrational thresholds of $NO^+(X\,^1\Sigma^+)$ obtained in the ab initio potential of [11]

v	E_t (eV)	Ref. [6]
1	0.288	0.290
2	0.572	0.576
3	0.852	0.859
4	1.129	
5	1.401	

[17,18] were obtained from these data using the relations

$$E_r = E_t - \varepsilon = E_t - \frac{1}{(n-\alpha)^2}, \quad \Gamma = \frac{2\beta}{(n-\alpha)^3} \qquad (3)$$

where all energies are in Rydbergs, E_t is the threshold to which the Rydberg series converges and n is an integer representing the principal quantum number of the Rydberg electron.

3. Results

3.1. Eigenphase sums

Eigenphase sums were obtained for the total symmetries $^2\Sigma^+$, $^2\Pi$ and $^2\Delta$. Fig. 1 presents the eigenphase sum obtained for the $^2\Delta$ total symmetry. Similar plots to this one have been drawn for the cases of $^2\Sigma^+$ and $^2\Pi$ total symmetries. The grid of energies used in the plots is 1×10^{-4} eV; as most of the resonances studied are narrower than this, they appear as discontinuities rather than jumps by π. The energy range studied is divided in 5 subranges by the NO^+ vibrational thresholds. The energy scale is the same in each subrange and the thresholds line up vertically on the right hand side of the panels. In this representation, members of a Rydberg series with the same n but associated with different vibrational thresholds align vertically. The fact that they move little between panels shows that the dependence of their quantum defects on the vibrational state is small.

In $NO^+(X\,^1\Sigma^+)$, $\Delta E_t \simeq 0.0213$ Ryd, so, from Eq. (3) we have that $\varepsilon < \Delta E_t$ when $n > 6.85 + \alpha$. For the series with $l \geq 3$, α is small ($< |0.05|$, see below), so Rydberg states with $n \leq 6$ do not appear as autoionizing states in the series converging to $v^+ = 1$. In the bottom panel of Fig. 1, we indicate the value of n after identification of the Rydberg series based

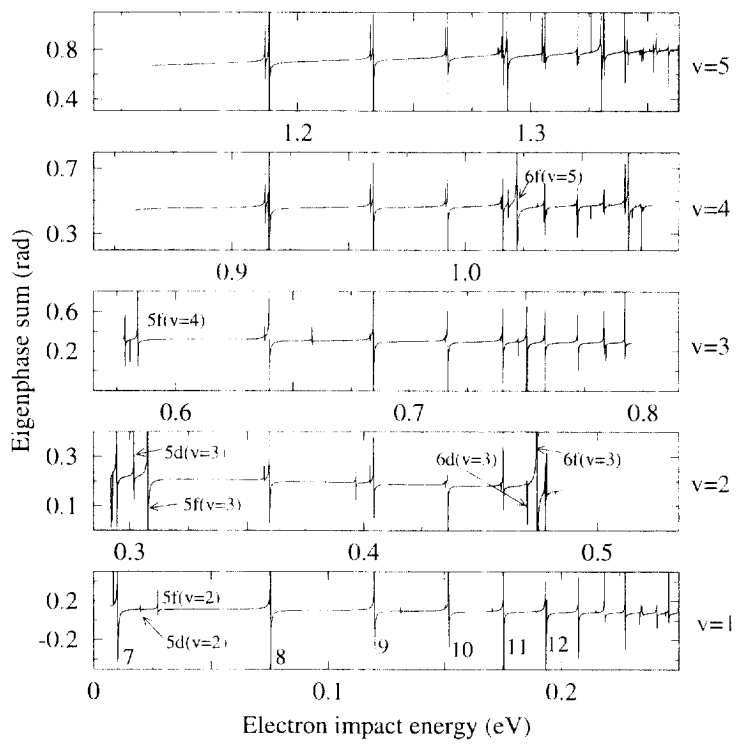

Fig. 1. Eigenphase sums for elastic electron–$NO^+(X\,^1\Sigma^+)$ scattering with total symmetry $^2\Delta$. Numbers in the bottom panel indicate the principal quantum number, n, of the fδ series of resonances converging to $NO^+(X\,^1\Sigma^+, v^+ = 1)$. Vibrational thresholds are aligned vertically on the right hand side of the panels.

on the quantum defect α obtained with Eq. (3) and comparing with values obtained in [10,11], where a partial wave analysis above threshold gave the l-composition of the series.

The strongest series of resonances is the fδ. Accompanying this one, at slightly lower energies, is the dδ series (not visible in the series converging to $v = 1$). Low-n (≤ 6) resonances associated with one vibrational threshold appear below a lower one. Some of these low-n resonances are identified in the panels with labels. Thus, in the lowest panels, resonances 5dδ and 5fδ to the $v + 1$ threshold appear between 7fδ and 8fδ to the v one, and the 6d,f$\delta(v + 1)$ resonances are between 11,12f$\delta(v)$.

In the experimental autoionisation spectra obtained by Ono et al. [6], the dδ series appears at lower energies than the fδ. Ono et al. recognised that the assignment of these series was uncertain because they always lie close to each other. Our calculations support Ono et al.'s assignment.

In the following subsections, we present quantitative information for the $^2\Sigma^+$, $^2\Pi$ and $^2\Delta$ resonance series. A convenient way of doing this is by plotting the quantum defect (the real part, α, and the imaginary part, β) as a function of the Rydberg energy ε (Edlèn [19] plots) of Eq. (3). These plots are compared with results from [11] at $R = 2.175\ a_0$, that do not include nuclear motion effects, and experimental results where available.

3.2. Series ns

Fig. 2 presents Edlèn plots of α and β for the ns Rydberg series. For this series α shows little dependence on v, but β clearly increases from the series $v = 1,2$ to $v = 3$ and to $v = 4,5$.

As shown in (3), β is related to the width of the resonances. We illustrate this relationship in the figures by plotting lines of constant width. The resonance width found for these series is in between 10^{-5} and 10^{-6} eV. Our results show that β increases with n and the resonances fitted show an approximate constant width as n increases.

Anezaki et al. [4,5], have measured the quantum defect of the ns Rydberg series to $v = 1$ from autoionisation spectra. The values, between $\alpha = 1.1$ and $\alpha = 1.2$ for members between $n = 8$ and $n = 15$, and, in particular, $\alpha_{13s} = 1.16$. As seen in Fig. 2, these values are in agreement with our results. However, while our α increases with n, theirs decrease.

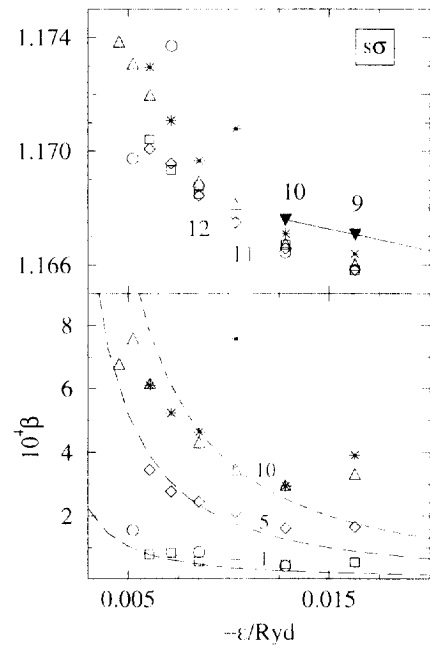

Fig. 2. Edlèn plots of the real (α) and the imaginary (β) quantum defects for the s Rydberg series of NO. The vibrational limits $NO^+(X^1\Sigma^+,v)$, of these series are: ○ $v = 1$; □ $v = 2$; ◇ $v = 3$; △ $v = 4$ and ∗ $v = 5$. Solid linked triangles correspond to a fixed-geometry calculation at $R = 2.175\ a_0$. In the upper panel, numbers indicate the principal quantum number n of the Rydberg states. In the lower panel, three lines represent constant resonant width with values indicated in μeV.

3.3. Series np

Fig. 3 displays α and β for Rydberg series pσ and pπ. In the pσ series, with the exception of the series to $v = 2$, of which only three members could be fitted, both α and β show a strong dependence on v. This dependence is largely monotonic, although the widths of the pσ series to $v = 5$ are between those to $v = 3$ and $v = 4$. The pπ series show a weaker and more mixed dependence on v, except for the α values of the series to $v = 1$ which are lower than the others.

In Fig. 3, it is apparent that the series of resonances do not follow the lines of constant width but, approximately, a linear relation between β and ϵ, as predicted by standard MQDT [17]. Resonance widths

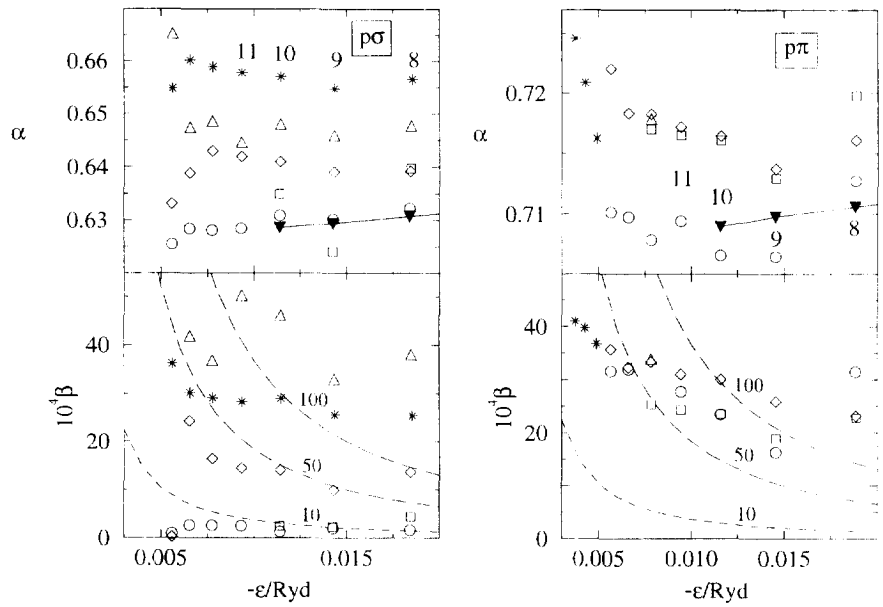

Fig. 3. Edlèn plots of the real (α) and imaginary (β) quantum defect for the pσ and pπ Rydberg series of NO. Symbols and numbers are as in Fig. 2.

in the p series vary between 10^{-3} and 10^{-5} eV. The fact that β is almost constant indicates that they get longer lived as n increases, as observed experimentally [5]. Our calculations show good agreement with experimental values in Fig. 8 of [4] ($\alpha_{p\pi} \simeq 0.72$, $\alpha_{p\sigma} \simeq 0.65$).

The width of the first members of the p series of resonances to $v = 1$ have been determined experimentally by Anezaki et al. [5] to be $\simeq 3 \times 10^{-4}$ eV. Using the experimental values of α, we can estimate values of β: $\beta_{8p} = 68$, $\beta_{9p} = 77$, $\beta_{10p} = 97$, $\beta_{11p} = 98$. Our results for pπ series to $v = 1$ are a factor of two smaller. This disagreement is not surprising since this is a case where predissociation determines the width of these states [5,8], and a good description would required the explicit inclusion of NO^+ excited states in the outer region calculations and the nuclear continuum.

3.4. Series nd

Fig. 4 shows Edlèn plots of the series dσ, dπ and dδ. The dπ and dδ series show a clear dependence on v. The same, although less clear, occurs in the dσ series. For the d series, as in the p series, β is almost constant with n and increases with v.

Our results show that the dπ and dδ series have similar widths (between 10^{-5} and 10^{-6} eV), while the dσ is broader (10^{-4} to 10^{-5} eV).

3.5. Series nf and ng

Fig. 5 displays the series fσ and fδ. Both show a clear progression in α as v increases. In the fδ case, it is noticeable that α is negative for the series converging to $v = 1$, in contrast to the positive value for the same series below other thresholds and the fixed-geometry results. Indeed, the fδ series crosses higher-l series as it moves from negative to positive values of α as v increases. These crossings make fitting the resonance difficult as the higher-l series appear within the width of the fδ resonances. The automatic fitting with RESON was completed and corrected with the more manual time-delay method [20].

The fδ series to $v = 1$ shows the biggest widths. Our results show that β decreases for v odd and increases for v even, approaching the widths, in both cases, of the series to $v = 5$.

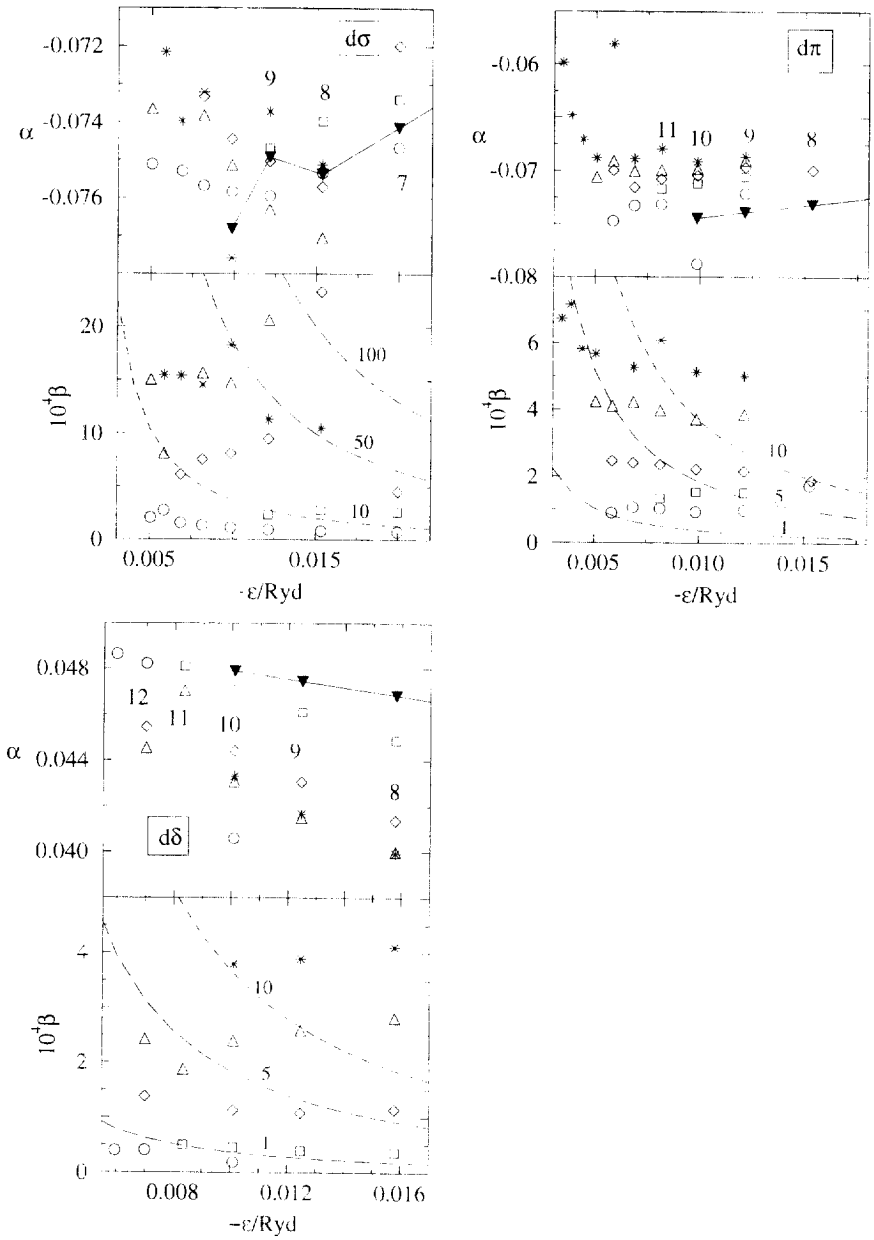

Fig. 4. Edlèn plots of the real (α) and imaginary (β) quantum defect for the dσ, dπ and dδ Rydberg series of NO. Symbols and numbers are as in Fig. 2.

Experimental values for the series to $v = 1$ are $\alpha_{12f} = 0.015$ [5], which agrees qualitatively with our values for $v > 1$.

Fig. 5 also gives Edlèn plots for the gσ series. This series shows strong dependence on v, especially for β. Series to $v = 2$ and $v = 3$ show a similar behaviour in α but differ strongly in β. This series also shows a great dependency of both widths and positions on n. Finally, we note that resonances with $l > 4$ were all very narrow.

3.6. Branching ratios of dδ and fδ series

Autoionisation branching ratios for the dδ and fδ series were calculated using the time-delay method [20] in order to compare with the experiment of Achiba and Kimura [3]. Our results are shown in Table 2. For the dδ series, the target states populated follow the propensity rule $\Delta v = -1, -3$. For the fδ series states $v = 0$ and 1 are mainly populated, except for the series to $v = 4$ which populates evenly all the available v states.

Achiba and Kimura suggested that the dominant

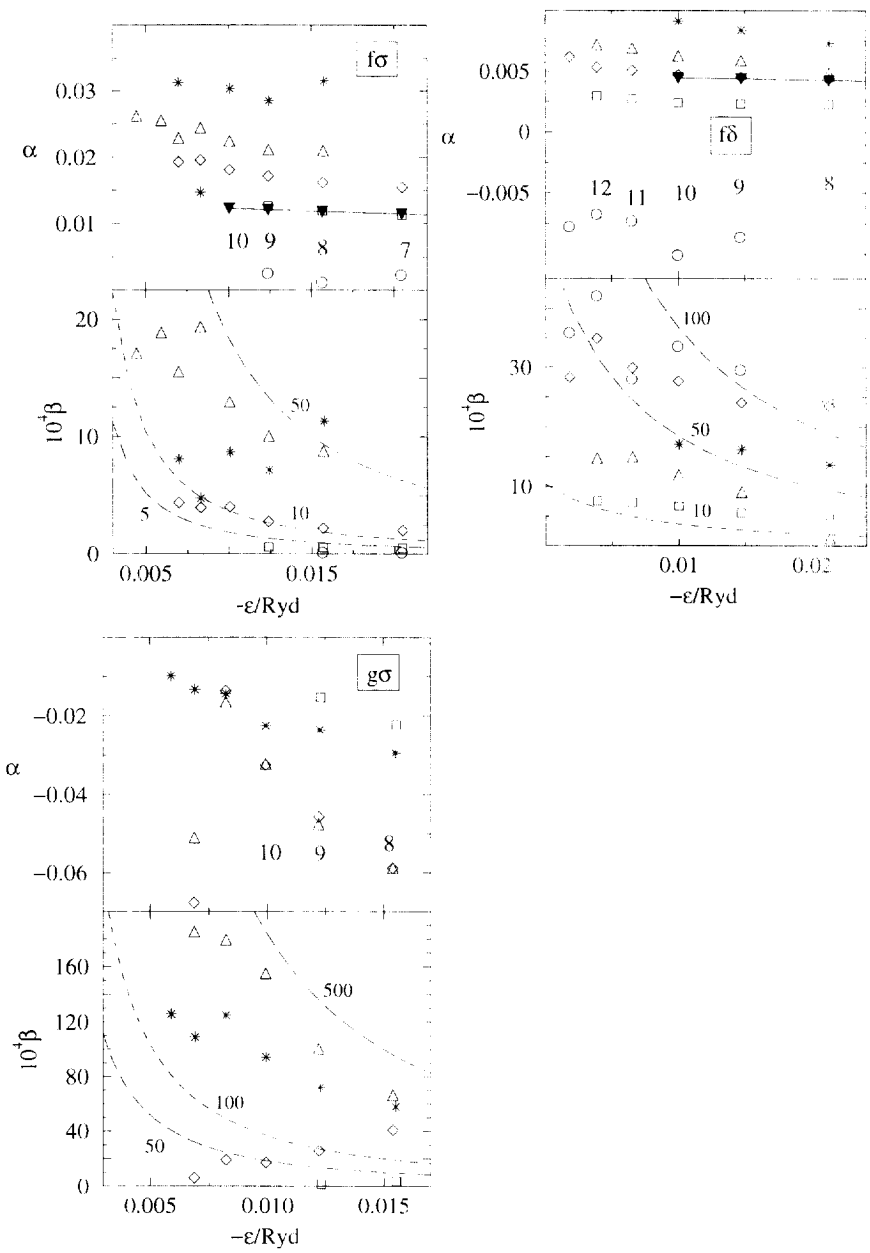

Fig. 5. Edlèn plots of the real (α) and imaginary (β) quantum defect for the fσ, fδ and gσ Rydberg series of NO. Symbols and numbers are as in Fig. 2.

Table 2
Autoionisation branching ratios of the d and f Rydberg series of $NO(^2\Delta,v)$ to $NO^+(X\,^1\Sigma^+,v^+)$ thresholds. Notation in the resonance column is $nl\lambda(v)$

Resonance	$v^+=0$	$v^+=1$	$v^+=2$	$v^+=3$	$v^+=4$
8d δ(2)	0.286	0.714			
9d δ(2)	0.399	0.601			
10d δ(2)	0.347	0.653			
11d δ(2)	0.523	0.477			
8d δ(3)	0.129	0.006	0.865		
9d δ(3)	0.274	0.031	0.694		
10d δ(3)	0.405	0.065	0.529		
8d δ(4)	0.002	0.071	0.012	0.915	
9d δ(4)	0.002	0.166	0.027	0.805	
10d δ(4)	0.001	0.232	0.031	0.731	
8d δ(5)	0.009	0.003	0.083	0.047	0.858
10d δ(5)	0.035	0.013	0.166	0.035	0.751
8f δ(2)	0.867	0.133			
9f δ(2)	0.871	0.129			
10f δ(2)	0.858	0.142			
11f δ(2)	0.764	0.236			
12f δ(2)	0.801	0.199			
8f δ(3)	0.553	0.431	0.016		
9f δ(3)	0.556	0.432	0.012		
10f δ(3)	0.550	0.438	0.012		
9f δ(4)	0.323	0.146	0.296	0.235	
10f δ(4)	0.382	0.169	0.349	0.100	
9f δ(5)	0.152	0.729	0.001	0.085	0.033
10f δ(5)	0.151	0.726	0.001	0.091	0.032

autoionisation route for the d δ(4) series is via the B' $^2\Delta$ valence state and results mainly in population $v=0$. We find $\Delta v=-1$ as the dominant autoionisation route, hence a dominating vibrational coupling between Rydberg states and ionisation continuum. We note that our outer region calculation omits electronic coupling to B' $^2\Delta$, which could be significant.

4. Conclusions

Non-adiabatic **R**-matrix calculations of resonance widths and positions for the autoionizing Rydberg series of NO converging to the first 5 vibrational thresholds of $NO^+(X\,^1\Sigma^-)$ have been presented for the total symmetries $^2\Sigma^+$, $^2\Pi$ and $^2\Delta$. The dependence of the series on the vibrational state of the target (v) is generally small (between 0.002 and 0.02, or 0.1% and 5%) in the real part of the complex quantum defect (α), while the imaginary part (β) can change by an order of magnitude between series to $v=0$ and $v=5$ (examples are series dσ, fσ, pσ, dπ).

The autoionisation widths of the resonances varies between 10^{-6} to 10^{-4} eV, depending on the symmetry of the series and the vibrational state of the target. Short lived resonances are seen in series p and f, while s and d are longer lived. NO has a large quadrupole and, if the quadrupole plays the main role in coupling the Rydberg states with the continuum, p and f on one hand and s and d on the other show similar widths. None the less, the width of the resonance decreases as the principal quantum number n of the Rydberg state increases; resonances with low n (<10) show autoionisation widths close to 10^{-4} eV.

In all cases, the non-adiabatic calculations and the fixed-geometry results of [11] are close, as can be expected due to the small dependence of the quantum defects α on the bond length (see Fig. 9 of [11]). There is also qualitative agreement with experimental results in [4–6].

For the dδ series, it was found that the $\Delta v=-1$ propensity rule seems to be valid, but not for the fδ series. Our results are not compatible with a Franck–Condon based selection rule [3] for branching ratios. However, this could be an artifact of our calculation due to the omission of excited target states in the outer region calculations.

Acknowledgements

This work was supported by the UK Engineering and Physical Sciences Research Council under grants GR/K47702 and GR/K89214.

References

[1] H. Park, D.J. Leahy, R.N. Zare, Phys. Rev. Lett. 76 (1996) 1591.
[2] J. Guo, A. Mank, J.W. Hepburn, Phys. Rev. Lett. 74 (1995) 3584.
[3] Y. Achiba, K. Kimura, Chem. Phys. 129 (1989) 11.

[4] Y. Anezaki, T. Ebata, N. Mikami, M. Ito, Chem. Phys. 97 (1985) 153.
[5] Y. Anezaki, T. Ebata, N. Mikami, M. Ito, Chem. Phys. 89 (1984) 103.
[6] Y. Ono, S.H. Linn, H.F. Prest, C.Y. Ng, J. Chem. Phys. 73 (1980) 4855.
[7] A. Fujii, N. Morita, J. Chem. Phys. 98 (1993) 4581.
[8] A. Giusti-Suzor, Ch. Jungen, J. Chem. Phys. 80 (1984) 986.
[9] H. Nakamura, Int. Rev. Phys. Chem. 10 (1991) 123.
[10] I. Rabadán, J. Tennyson, J. Phys. B: At. Mol. Opt. Phys. 29 (1996) 3747.
[11] I. Rabadán, J. Tennyson, J. Phys. B: At. Mol. Opt. Phys. 30 (1997) 1975.
[12] C.J. Gillan, J. Tennyson, P.G. Burke, in: W.M. Huo, F.A. Gianturco (Eds.), Computational methods for electron-molecule collisions, Plenum Press, New York, 1995, p. 239.
[13] C.J. Gillan, O. Nagy, P.G. Burke, L.A. Morgan, C.J. Noble, J. Phys. B: At. Mol. Opt. Phys. 20 (1987) 4585.
[14] B.I. Schneider, M. Le Dourneuf, P.G. Burke, J. Phys. B: At. Mol. Opt. Phys. 40 (1979) L365.
[15] R.J. Leroy, University of Waterloo Chemical Physics Research Report, CP-555R, 1996.
[16] J. Tennyson, C.J. Noble, Comput. Phys. Commun. 33 (1984) 421.
[17] M.J. Seaton, Rep. Prog. Phys. 46 (1983) 167.
[18] D.L. Moores, H.E. Saraph, Atoms in Astrophysics, Plenum, New York, 1983.
[19] B. Edlèn, Handbuch der Physik, Springer, Berlin, 1964.
[20] D. Stibbe, J. Tennyson, J. Phys. B: At. Mol. Opt. Phys. 29 (1996) 4267.